Controlled stacking for improved quality of prestack depth-migration results

DAVID KESSLER, CGG American Services, Houston, Texas
LUIS CANALES and CHUNG-CHI SHIH, CogniSeis Development, Houston, Texas
PETER DUNCAN, 3DX Technologies, Houston, Texas

Depth migration of seismic data is becoming more routine for imaging of complex geological structures. However, in some cases, the quality of the resulting depth section is lower than expected. A typical case is in imaging of salt bodies. The seismic images of steeply dipping salt flanks are frequently broken, smeared, and difficult to interpret. The study presented in this paper demonstrates one source of this imaging problem, and suggests a solution we call *controlled stacking*. The core of the solution is the correct muting of partial images produced by prestack depth migration (preSDM) before sorting and stacking to obtain the final depth section.

Our investigation started with the processing of a 3-D seismic dataset acquired over a massive salt dome (Figure 1). The geological objective of the exploration project was to define the position of the sediment/salt interface as accurately as possible to allow placement of drilling locations high on the producing horizons. Evaluation of a geometric reservoir model in this area helped to set the processing goal: a lateral resolution of 100 ft on the seismic image. This level of accuracy is needed to direct a well to the top of a producing layer, and still be at a safe distance from the salt face.

Strong lateral velocity variations and steeply dipping salt flanks led to the selection of 3-D DMO followed by 3-D poststack depth migration (postSDM) as the imaging tools. Sixty wells in the survey area were used to generate a 3-D velocity model and calibrate the seismic depth volume. Working layer-by-layer in a constant velocity half space (CVHS) mode of operation, as discussed by Kessler et al. in "Depth processing: An example" (*TLE*, 1995), nine layers were constructed, eight at sedimentary layer boundaries and the ninth at the salt/sediment interface. While constructing the velocity model and forming the seismic image, we confirmed that the image tied the formation tops selected from the well data. Following processing, the resultant seismic depth volume was loaded onto a workstation for final interpretation (Figure 1). The objective at this stage was to accurately interpret the salt shape.

Two problems were encountered while analyzing the seismic volume and well data in detail. First, in spite of using a steep dip and high-fidelity depth migration algorithm, the salt flanks were hard to pick since the quality of the salt reflection was fairly poor. Second, at places where the wells reached the salt, we found

I must be in the wrong part of TLE*, you say as you look at the title of this paper. Isn't this supposed to be Interpreter's Corner, that part of* TLE *which focuses on extracting geological meaning from geophysical data? Well, this is Interpreter's Corner, so what is the paper by Kessler et al. doing here?*

Traditionally, geophysics has been divided into acquisition, processing, and interpretation/mapping. We seismic interpreters would typically lay out (2-D) lines on a map and then let the acquisition and processing experts do their jobs. Upon receiving the final processed data, we would begin interpreting. We used geological expertise and insight to try to understand what was happening between widely spaced, variable quality, lines. This was followed by depth conversion using limited velocity information and, finally, hand contouring. Since our information was sparse and we understood the limitations of our data, we had ample opportunity to introduce our geologic and interpretive influence.

With the arrival of high-quality 3-D data, we no longer had to guess what was happening between lines and, say, which faults connected with which. Due to the continuous spatial coverage and improved imaging, we could frequently define an unambiguous time picture. However, we could still apply our geological insights and influence during the depth-conversion stage since velocity data remained sparse and less-than-perfect.

Now, as the industry generates significant amounts of depth data, the interpreter has essentially no room to impose geologic influence if he or she works in the traditional way. This is not because depth conversion has suddenly become more precise (although the imaging has). Rather, the point at which geologic insight is applied has been moved a step.

If the "traditional" approach is used, then processors of the data are the de facto interpreters since they make the key decisions that control the final depth section. Those with the title of interpreter are relegated to pickers and map makers.

I suspect that few interpreters will accept this situation. Thus, the increased use of depth imaging means that interpreters will have to gain a better understanding of processing and will have to approve key decisions made during the processing sequence. In fact, to avoid interpretation being done by the processor, the interpreter will (almost) have to become a processor.

Perhaps now you will see why we will occasionally have papers in Interpreter's Corner that look as if they have come straight from TLE*'s Acquisition/Processing section. The benefit to interpreters of the following paper is that it shows the difference in application and results of a poststack migration approach and a prestack migration approach in a salt-dome setting, and it also shows how imaging of salt/sediment geometry can be improved by the use of new processing techniques. When you start working on your next salt-flank prospect, you'll be glad you read this paper.*

Allen Bertagne
TLE Editorial Board

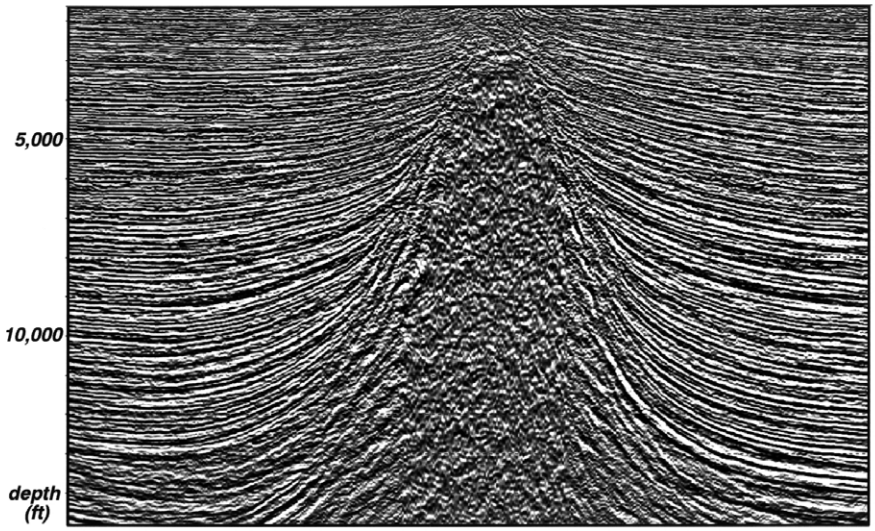

Figure 1. Subline 300 of the seismic volume after the last iteration of postSDM. These data are used for the final interpretation of the salt body.

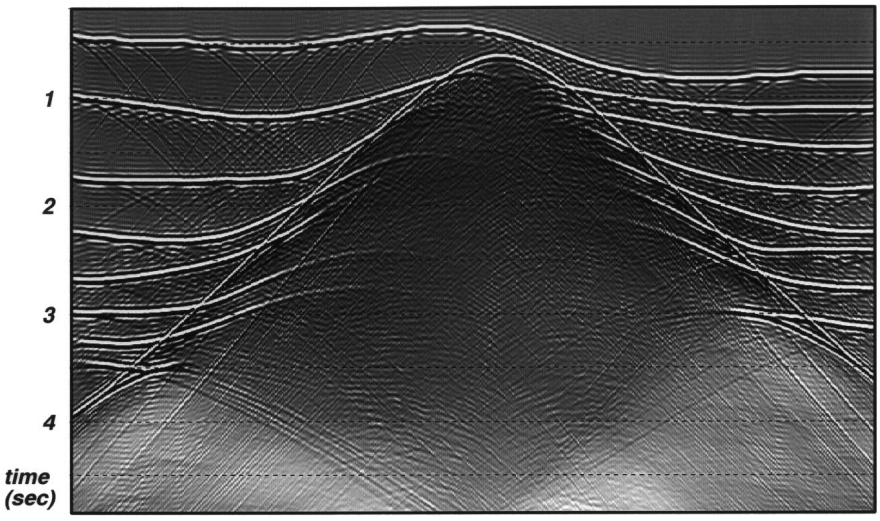

Figure 2. Zero-offset section produced using the exploding reflector concept. The numerical modeling scheme used in generating the synthetic data is based on a pseudo-spectral algorithm, as introduced by Kosloff and Baysal in "Forward modeling by the Fourier method" (GEOPHYSICS, 1982).

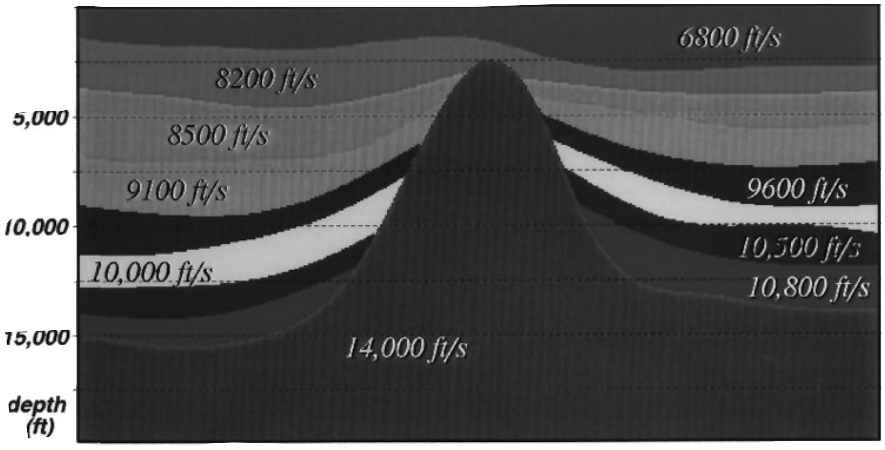

Figure 3. Subsurface velocity model used for creation of the synthetic data. The surfaces, velocities, and acquisition parameters are the same as for the field dataset.

the salt interface to be mispositioned even when formation tops tied the seismic reflections at nearby well locations.

Exploding reflector modeling. To understand the source of the salt flank imaging problem using the processing flow described above, synthetic seismic data were generated. Using the *exploding reflector concept*, a modeling and migration rule developed by Loewenthal et al. (see "The wave equation applied to migration, *Geophysical Prospecting* 1976), a 2-D zero-offset section was generated (Figure 2). Inline 300 from the velocity volume was selected as the 2-D velocity model (Figure 3).

Comparison of the synthetic section to the field data (Figure 4) reveals that the two sections have similar characteristics. The salt dome creates a large area of incoherent signal, surrounded by reflections from the sedimentary layer boundaries. The main difference between the synthetic zero-offset section and the field data is the strength of the salt flank reflections. This difference exists because the numerical data are generated using the 2-D wave equation, whereas the field data demonstrate the more realistic decay of amplitude in a three-dimensional world.

Depth migrating the numerically modeled section, we obtain a very accurate depth image (Figure 5) which matches the exploding reflectors very well. From this experiment, we learn that for the salt dome structure model presented in Figure 3, a true zero-offset time section can be migrated to depth to obtain a very satisfying result. Why, then, are the results of the same migration algorithm not as good when applied to the real data?

Wavefield analysis. One of the advantages of numerical modeling is the ability to generate wavefront snapshots. They can be used to analyze and understand wave propagation phenomena.

Using the model shown in Figure 3, we located a shotpoint above the salt structure and generated wavefront snapshots at different propagation times (Figure 6).

Analyzing these figures, we learn about the partitioning of energy in the vicinity of the salt dome. The steep angle of the salt flank and the large difference in velocity between the salt and the surrounding sedi-

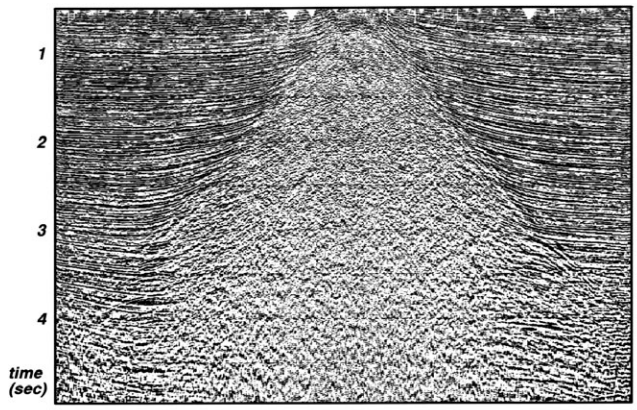

Figure 4. Subline 300 of the DMO-stack volume. This section can be compared to the synthetic zero-offset section shown in Figure 2.

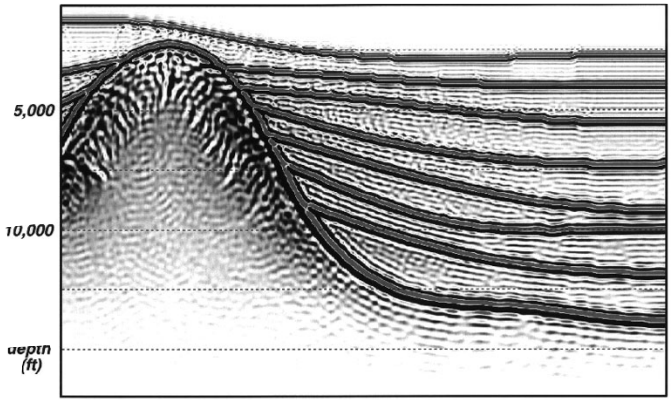

Figure 5. PostSDM result of the numerically modeled zero-offset section. The migration algorithm is based on wavefield extrapolation in the (w,x) domain.

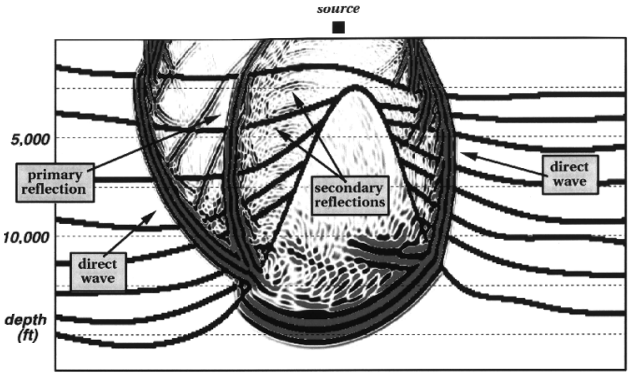

Figure 6a. Wavefield snapshot at 1.5 s. Secondary reflections are generated at the salt/sediment terminations and start to propagate upward.

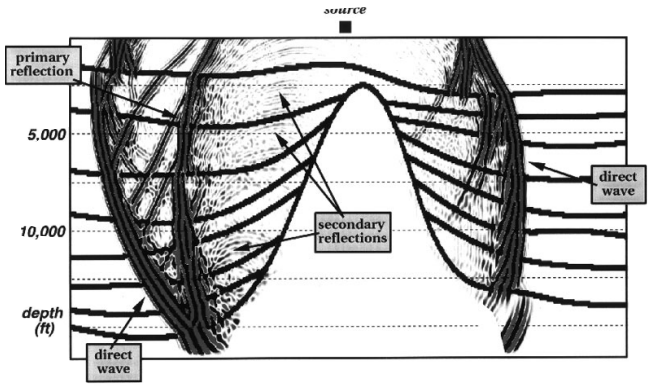

Figure 6b. Wavfield snapshot at 2.0 s. The secondary reflections are propagated upward and recorded at the receivers as hyperbolic events.

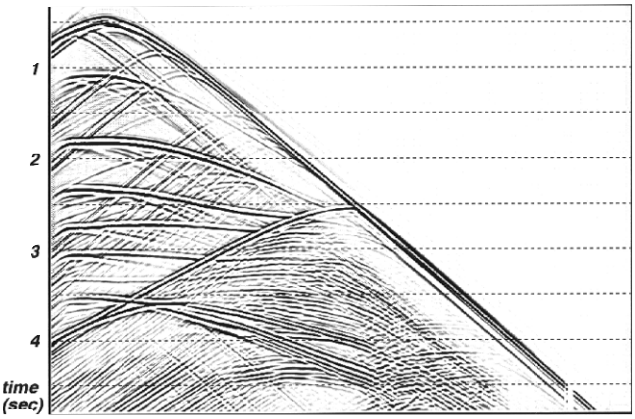

Figure 7. A shot gather produced by the numerical simulation. Acquisition parameters for generation of the prestack synthetic data are the same as those used in recording the field data. The group interval is 82.5 ft. and the shot interval is 330 ft.

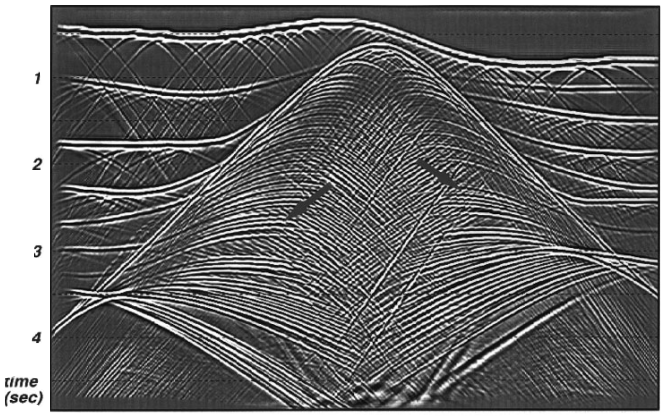

Figure 8. DMO-stack section resulting from processing the synthetic dataset. Secondary reflections are marked by the red arrows.

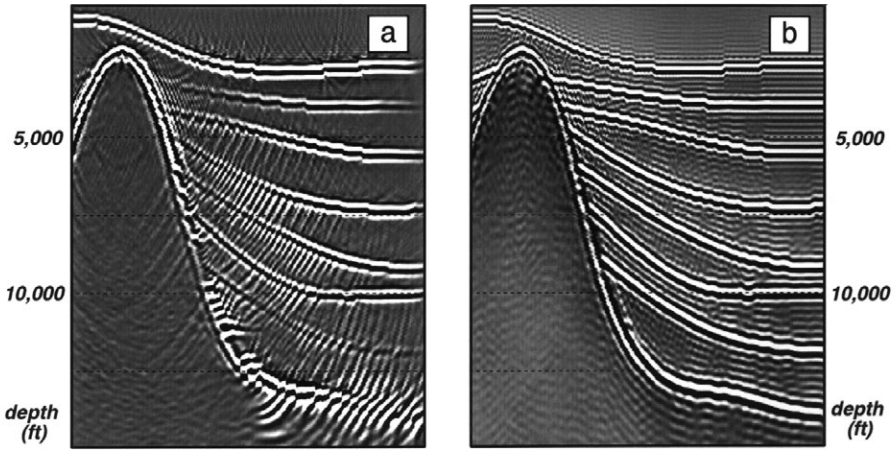

Figure 9. (a) PostSDM of the DMO stack section. (b) PostSDM of the zero-offset section. Destructive interference of the direct salt reflection and the secondary reflections deteriorates the salt flank image.

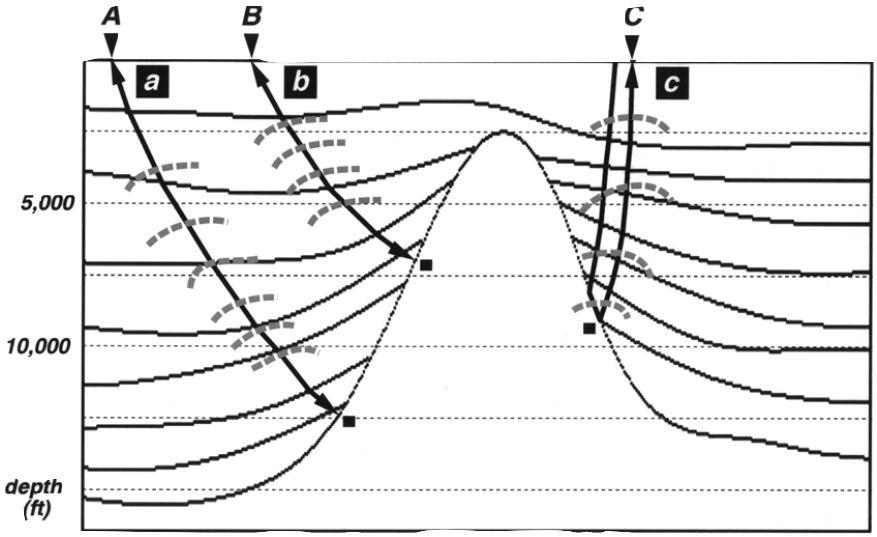

Figure 10. Source location and reflection point combination for raypaths a and b obey the exploding reflector concept. The raypath of the downgoing wavefront is identical to the raypath of the upgoing wavefront. For raypath c, the downgoing path differs from the upgoing path. Thus energy recorded at receiver C cannot be imaged correctly using the one-way donward propagation solution. Reflection points are marked by black squares.

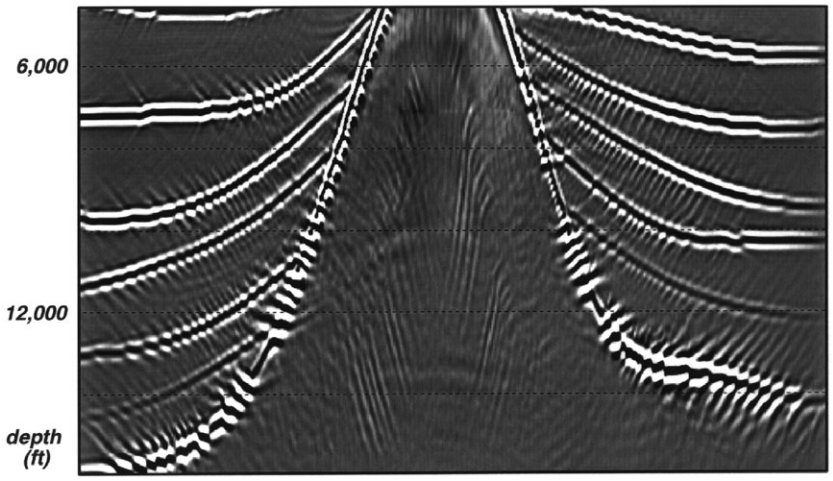

Figure 11. PreSDM result. Depth migration was applied in the shot domain using a Kirchhoff summation algorithm.

ments create a wave guide along the salt flanks. Energy propagating along the salt flanks encounters the sedimentary interfaces on its way down. At each location where a sedimentary layer is reached, a secondary wavefront is generated. These wavefronts propagate upward in the sedimentary portion of the subsurface and are recorded as hyperbolic events in the recorded shot point gathers. As described in the next section, the destructive interference of these secondary reflections and the primary salt reflections is the source of the imaging problem.

Shotpoint modeling and processing. The last step in our numerical modeling study was to produce a full set of 2-D prestack data. To generate the most realistic shotpoint gathers possible, a data generation scheme called a *moving shotpoint* was chosen. With this scheme, each numerical experiment is performed using the whole model, and only the shotpoint slides along the surface of the model. This provides two advantages; first, we avoid problems of boundary reflections and, second, we record events generated outside the cable area.

A typical numerical shot gather is shown in Figure 7. One hundred shotpoint gathers were generated, providing coverage for the entire model. The data were processed using the same flow used for processing the field data. Time processing results (a DMO stack section) are shown in Figure 8. Comparison of the DMO section to the synthetic zero-offset section (Figure 2) reveals that, on the former, reflections generated at the sediment/salt terminations have a stronger appearance.

Depth migration of this DMO stack section results in the section shown in Figure 9a. Two different events, the direct reflection from the salt and the secondary reflections from the salt/sediment terminations, try to migrate to the same location. The image of the salt flank is clearly inferior to the result obtained by the depth migration of the zero-offset section (Figure 9b).

Controlled stacking. The reason for the poor image quality of the salt flank is the destructive interference between the direct salt reflection

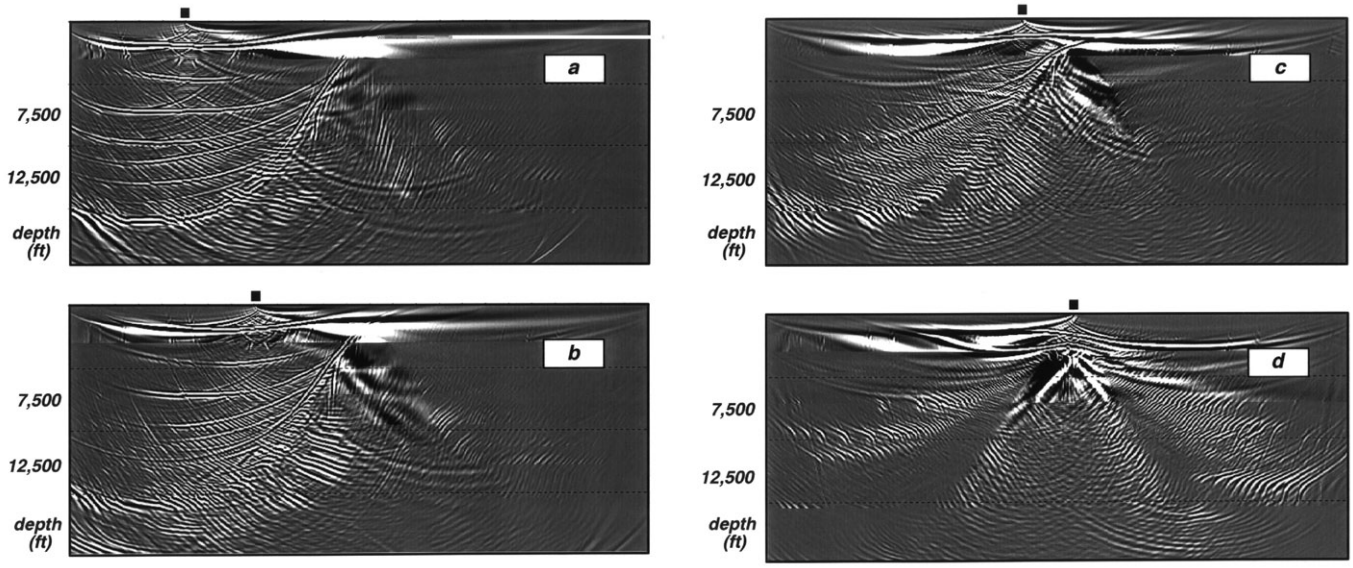

Figure 12. Partial images of the subsurface obtained by the application of preSDM in the shot domain. (a) Shot point 107. (b) Shot point 167. (c) Shot point 227. (d) Shot point 271. Shot points are marked by black squares.

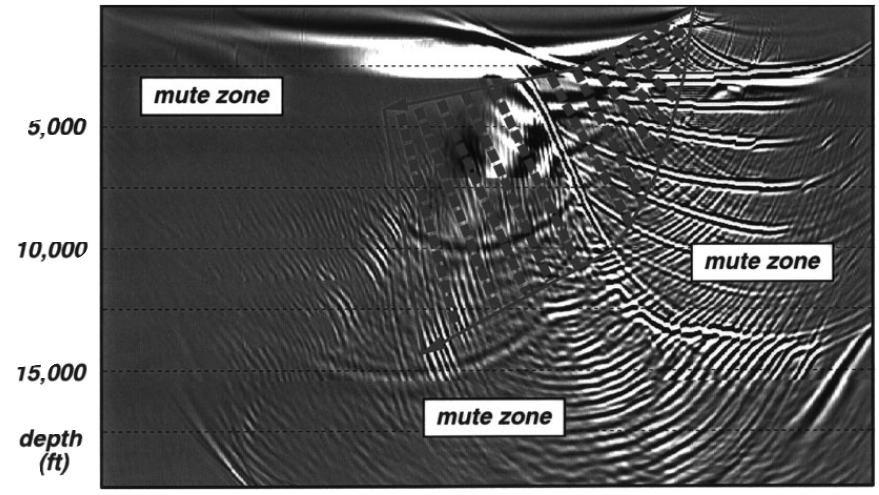

Figure 13. Controlled stacking is based on the selection of the subcritical zone of the partial image obtained by preSDM. This can be done using an automatic procedure based on a ray-tracing algorithm.

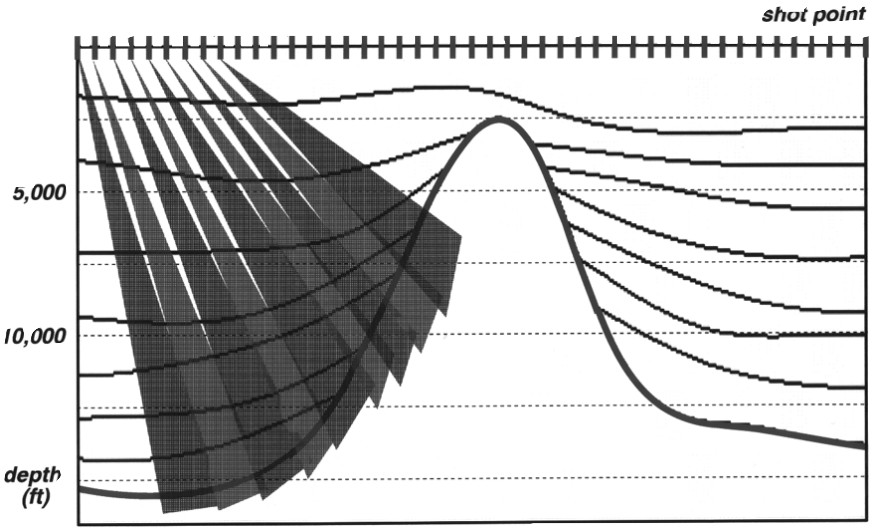

Figure 14. Based on the model geometry, the final image is constructed in segments selected from each partial image.

and the secondary reflections generated by the wavefront traveling down the salt interface; however, the problems are more significant. Even at places where the salt flank reflection can be traced, the position of the flank is not correct. The reason for the misposition is the algorithmic application of postSDM. Invoking the exploding reflector model as the imaging principle, we use the one-way wave equation to downward extrapolate the recorded wavefield. This assumes that the path of the upward propagating wavefield is identical to the path of the downward propagated wavefield. For wave fronts that reach the salt normal to its surface (cases a and b in Figure 10), the exploding reflector concept is obeyed. That is, the wave path in the downward direction is equal to the wave path in the upward direction. But in cases where the wavefront intersects the salt flank at overcritical angles (case c in Figure 10), they first refract along the salt flank, and then reflect back from the next salt/sediment termination. Since the downgoing path of this wavefront is different from the path of the upgoing wavefront, the exploding reflector concept is not obeyed, resulting in mispositioning of the salt flank reflections.

Use of preSDM instead of postSDM solves the positioning problem, but the poor salt flank image quality caused by the destructive interference of the two wavefronts remains (Figure 11). Nevertheless, the solution to the imaging problem

of the steep salt flanks can be achieved using a preSDM-based technique. When preSDM is applied in the shot domain (Figure 12), each migrated shot gather represents a partial image of the subsurface. Furthermore, since each shot gather has a different source position, each partial image illuminates the subsurface from a different angle. Analysis of the partial images shown in Figure 12 shows that each one contains a clear image of a different portion of the subsurface, especially of the salt flanks. To improve the quality of the final depth image, we need to apply controlled stacking to isolate and include only the desirable reflections from each of the partial images before sorting and stacking the data to obtain the final depth image.

Muting of partial images to retain the primary salt reflections can be done manually by inspection in processing of 2-D data; but to be practical in a 3-D environment, an automatic procedure should be applied. Having a rough estimate of the salt structure, we can submit a fan of rays through the model in order to find the two specific rays that reach the salt flank at critical angles, both in the up-dip and down-dip directions (Figure 13). Using these two special raypaths, a mute window is constructed, eliminating all the energy in the overcritical zone and leaving the energy that is imaged in the subcritical zone. Progressing shot-by-shot, the salt flank image is constructed piecewise, where each pass window consists of direct arrival energy (Figure 14).

Applications of the controlled stacking technique to the numerically generated full offset dataset produces the depth section shown in Figure 15. In this depth image, as compared to Figure 11, the salt flanks are clear, continuous, and easy to interpret. Furthermore, the salt body is constructed using primary arrivals only, and is positioned in its true vertical as well as horizontal location.

Field data example. A deep-water, marine 2-D dataset was available for the application of controlled stacking. Figure 16 shows the DMO stack section of this survey. The processing objective was to image, as accurately as possible, the salt body located at the center of the section shown in Figure 16. Application of postSDM

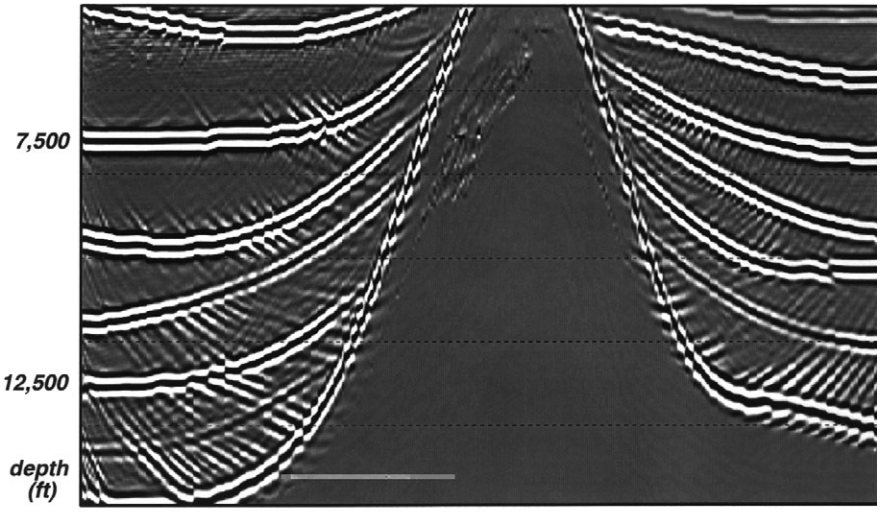

Figure 15. Final depth section obtained by preSDM and controlled stacking.

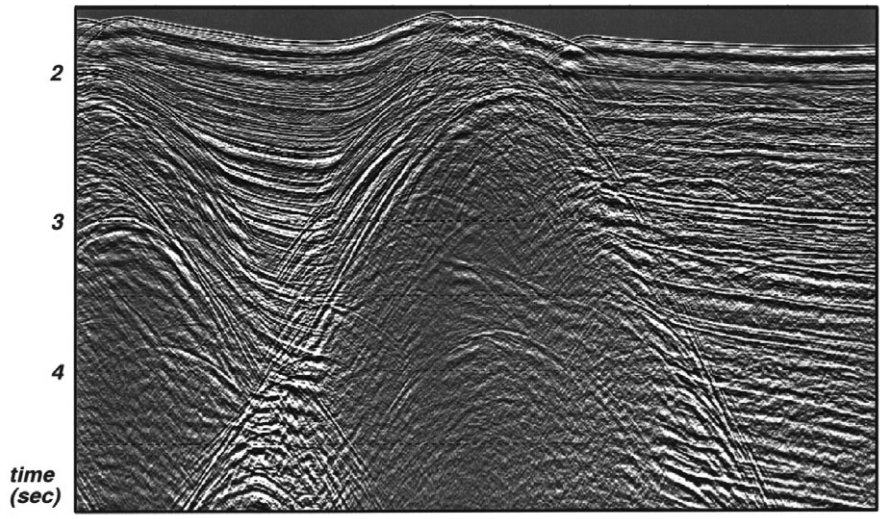

Figure 16. A DMO stack section of a deep-water, marine dataset used for application of controlled stacking.

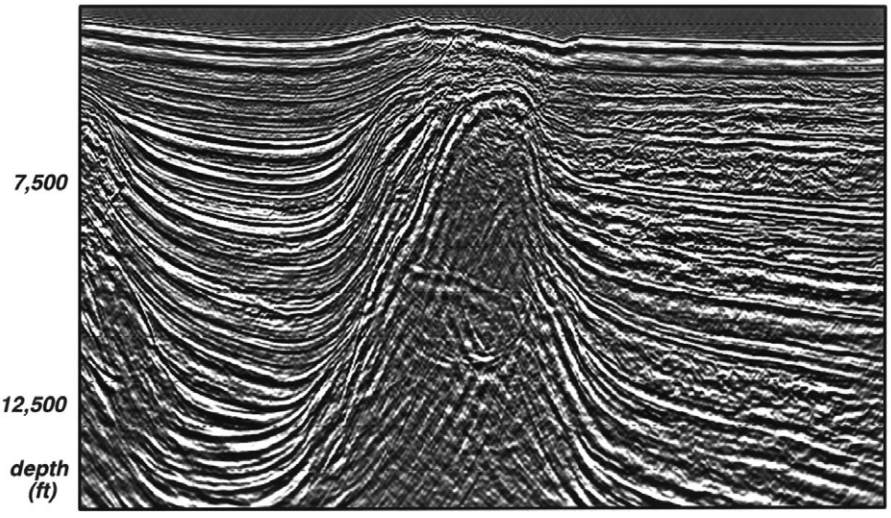

Figure 17. PostSDM result of the DMO stack section. The image of the right salt flank can be improved by controlled stacking.

produces the depth section shown in Figure 17. The image of the salt body is well defined on the left flank, but is poor on the right flank. The difference in salt flank imaging quality results from a t_o difference in the geometry of the sedimentary layers on the two sides of the salt body. The sedimentary layers on the left are pulled up close to the salt, and are almost parallel to the salt flank. On the right side, the sedimentary layers terminate at a larger angle against the salt flank. The poor quality of the salt flank image on the right is caused by the destructive interference of the primary reflected signal with secondary reflections generated at subsurface termination points. The image position is incorrect because the exploding reflector principle was violated.

Implementation of controlled stacking begins with application of preSDM. Figure 18 shows one of the partial images obtained by preSDM. This figure demonstrates the sensitivity of imaging the salt flank reflection. If not muted properly, stacking with the next partial image will deteriorate the image quality instead of improving it. The velocity model that is needed for processing is developed using the CVHS technique. Two image gathers resulting from the velocity analysis are shown in Figure 19. The velocity model is also used to isolate primary reflected energy for application in controlled stacking. The resulting depth section is shown in Figure 20a. The salt flank image, obtained by controlled stacking, is much easier to interpret than the one obtained from postSDM (Figure 20b). This comparison shows that, in some cases where postSDM is routinely used as the imaging tool, a preSDM-based technique is needed in order to achieve a correct and clear image of the subsurface.

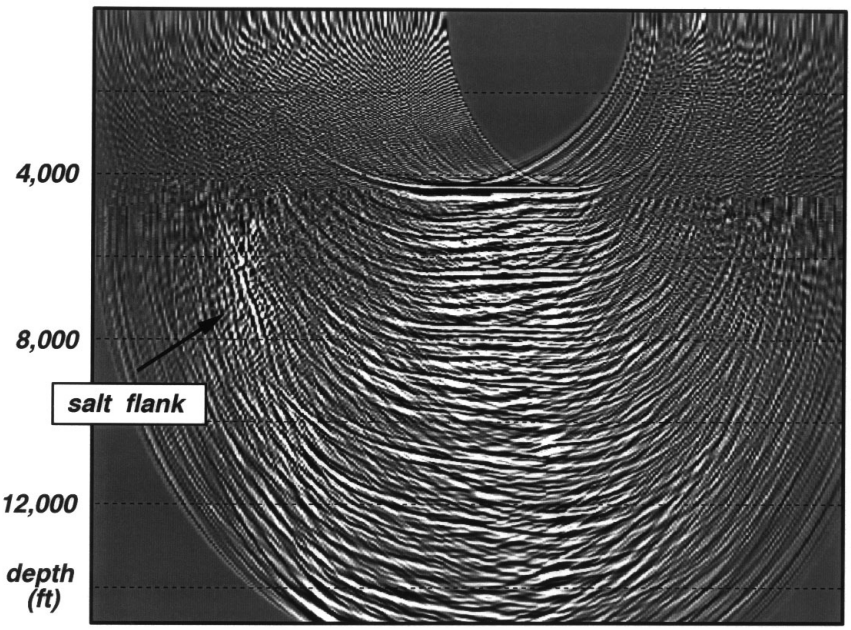

Figure 18. Partial image obtained by preSDM. Overstacking of the salt flank reflection will deteriorate the final image of the salt flanks. Controlled stacking is constructed to ensure the correct muting of partial images prior to stacking.

Summary. PreSDM, not postSDM, needs to be used when migrating a complex wavefield recorded over

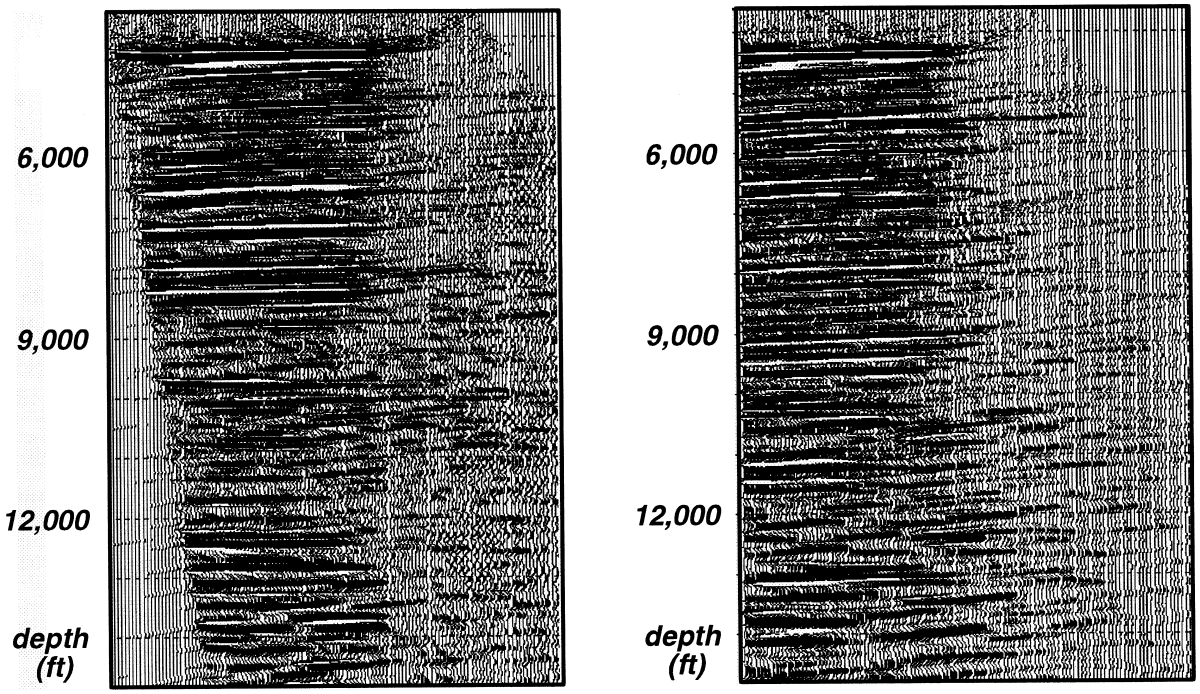

Figure 19. Common reflection point image gathers obtained from the migration velocity analysis procedure. The CVHS method was used for construction of the velocity model.

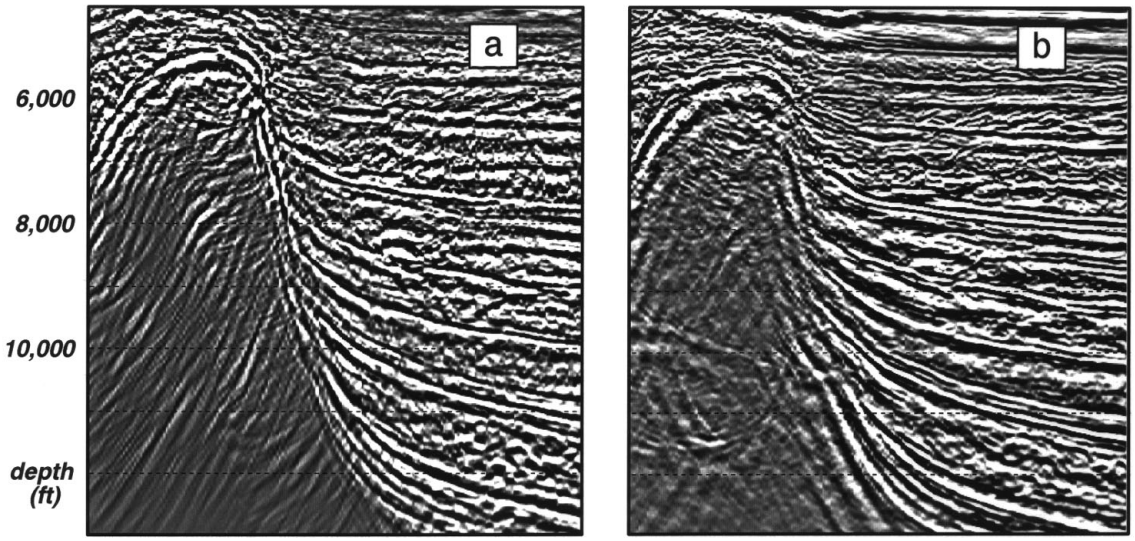

Figure 20. (a) Depth section obtained by controlled stacking. (b) Depth section obtained by postSDM. The preSDM algorithm is based on the Kirchhoff summation methoid. The postSDM algorithm is based on wavefield extrapolation in the (w,x) domain.

steeply dipping structures associated with lateral velocity contrasts. The advantage of preSDM processing is in the ability to isolate the appropriate portion of each partial image before stacking. This controlled stacking results in superior images of steeply dipping reflections such as salt flanks.

The process of controlled stacking belongs to a family of model-based procedures. With a good estimate of the subsurface velocity model, enhanced processing algorithms can be developed and applied, resulting in a better final product. In our study, we have shown the application of the technique for improved imaging of salt flanks. This controlled stacking can also be applied to other exploration objectives such as the imaging of steep fault planes.

Finally, we started our investigation with imaging problems encountered in the processing of a 3-D dataset, but demonstrated the controlled stacking procedure on a 2-D dataset. We believe that our method will be applicable for processing of 3-D datasets as full volume 3-D pre SDM becomes more routine. LE

Acknowledgments: We would like to thank Duane Dopkin and Paula Criswell for their reviews of the manuscript. Mike Plumlee is acknowledged for his help in processing the 3-D dataset.

Corresponding author: D. Kessler, phone 713-784-0740, email kessler@us.cgg.com